# DC Microgrid Protection in the Presence of the Photovoltaic and Energy Storage Systems

A. Shabani, K. Mazlumi*

*Department of Electrical Engineering, Faculty of Engineering, University of Zanjan, Zanjan, Iran.*

**Abstract-** *In recent years, most of the loads and distributed generations are connected to the AC grid through the power electronic converters. Using the DC grid beside the AC grid can reduce the conversion stages and power losses. Protection of the DC grids is a challenging issue because of the new structures of DC grids and fast transients of the DC faults. This paper studies the protection of the low voltage DC (LVDC) system in the presence of the photovoltaic (PV) and energy storage systems (ESS). An LVDC system consisting of a DC microgrid is considered and Different operating modes are analyzed. DC faults behavior and protection challenges are discussed for each mode through simulations employing MATLAB software. Finally, some methods are presented to solve the protection challenges. The results show that changing the protection arrangement of the system and choosing suitable control logics for the ESS and the PV prevent the unwanted outage of the loads and provide the possibility of the microgrid operation in islanded mode.*

*Keyword:* DC microgrid, ESS, Protection, PV, Switching logic.

## 1. INTRODUCTION

High growth rate of the electrical energy demand, limitation in fuel sources and environmental problems lead to high penetration of renewable energies and small scale units in the recent electricity network. These units can be efficiently utilized for changing the configuration of the generation system from centralized to distributed. This resulted in the emergence of "active" distribution systems and microgrids. Microgrids are local energy networks that involve renewable energy sources and storage systems. They have the capability to be locally controlled. Therefore, they can disconnect from the grid when there is a fault at the main grid, and continue to supply a portion of their local loads in a so called "islanded mode"[1].

Renewable and small scale units such as wind, photovoltaic, fuel cell, micro-turbine and combined heat and power (CHP) may generate DC voltage or AC voltage with different magnitudes and frequencies. Therefore, they need power electronic converters to be integrated with the existing power grid [2-4]. On the

other hand, most of the consumers such as telecommunication systems, traction systems, households, and office equipment are based on the DC systems. Devices such as computer, TV, fluorescent lamp have a rectifier in their configurations. Therefore, the integration of the low voltage DC system with the AC distribution system can reduce the number of converters [5-7]. The LVDC system is a suitable and more cost effective option for existing medium voltage AC (MVAC) distribution system [8], [9]. To increase the reliability of the LVDC system, it must be connected to the AC grid through a controlled voltage source converter (VSC) which provides bidirectional power flow [10].

Renewable sources change the configuration of the LVDC system and its performance. Because of non-deterministic generation of the renewable sources such as PV and wind turbine, the energy storage systems with different technologies are used in the AC/DC microgrids configurations for energy management, i.e., load levelling or peak shaving, for power bridging, and for power quality improvements. Energy management functions compared to the other functions require the energy storage systems to serve for long duration. Power bridging functions require energy storage systems to serve for few seconds to few minutes. For power quality improvements, the energy storage systems are required for only fractions of a second [11-16].

In recent years, a lot of work is being carried out on the

operation and control of the AC/DC microgrids. References [17-21] present a proper energy management system for a reliable operation of renewable sources and energy storages in a DC microgrid. Different operating modes of AC/DC microgrids and control strategies of energy storage systems have been studied in [22-25]. One area which needs more attention is the protection of the DC microgrids and power quality issues. On the other hand, progress in the energy storage technologies helps us use them for short-term applications such as transients and power quality improvements.

A brief review of DC microgrids in [26] demonstrated that the fault characteristics and protection requirements are different for DC and AC systems. The effect of short lines/cables and fault resistance can make protection of DC microgrids more challenging than that of AC microgrids.

DC faults occur in cables of the LVDC system for some reason such as failure of cable insulation or damaged cable caused by electrical stresses, environmental conditions, aging and physical damages [27-29]. The DC faults can be categorized as pole-to-ground fault and pole-pole fault depending on if one line is short-circuited to the ground or two lines are short-circuited. Faults on DC lines are usually pole-to-ground faults. A pole-to-pole fault seldom occurs because it requires a severe insulation damage of both positive and negative conductors [29-31]. DC fault current has large amplitude and transient that can damage the converter and the equipment close to it [32-33]. Although there are certain differences between the fault characteristics and topologies of DC microgrids and AC microgrids, the conventional protection principles are expected to be the main options available to protect DC microgrids. The overcurrent (O.C) relays are used in [34-35] for LVDC system protection. However, due to the high raising rate of DC fault currents, the coordination of O.C relays is a challenging issue and high speed measuring and protective devices are required. Differential method is suggested in [36-37]. In differential-based methods, the synchronization of current measurements under high di/dt, comparison of them and sending trip signal within required time frame are the main challenges. Therefore, this method needs advanced communication devices and costly synchronized measurement devices. The distance based method is used in [28] for fault detection and location purposes in DC networks. However, fault impedance especially for short cables negatively impacts the accuracy of this method.

The aforementioned methods need to be modified to

consider the effects of the renewable energy resources as well as some unique characteristics of DC microgrids on the system protection. Fault analysis of an active LVDC distribution network is presented in [38]. However, protection of the proposed network is not investigated as a DC microgrid. Protection of photovoltaic based DC microgrid is studied in [39] using differential protection method. Islanded mode of microgrid and different operating modes of PV and ESS are not considered in this method.

Most of the research in the field of the LVDC system protection has focused on the characteristics of the DC faults, new technologies of the protective devices and protection schemes design. However, protection of the LVDC systems in the presence of the renewable sources has not been studied sufficiently in the literature.

In this paper, protection of the DC microgrid in the presence of the PV and the ESS is investigated. Also, different operating modes of the system, the islanded mode of the microgrid and switching logics of the ESS are discussed from the system protection point of view.

The paper is organized as follows: Firstly, a low voltage DC distribution system is considered and its protection is studied. Secondly, a PV unit is added to the LVDC system and its effects on the protection scheme are investigated. Thirdly, by adding the energy storage system to the LVDC system, possible operating modes of the DC microgrid in the fault condition are considered. Then, effects of each case on the fault transients are studied through simulations. Finally, a switching logic is proposed for the energy storage to mitigate the fault transients and its performance is discussed in the fault condition of the system.

## 2. SYSTEM CONFIGURATION AND OPERATION

### 2.1. LVDC system structure and circuit configuration

The investigated LVDC system layout is shown in Fig. 1. It is connected to the AC grid through a bi-directional AC/DC converter called VSC which enables power flow in two directions. Within the LVDC system, a DC microgrid consisting of a PV, an energy storage system, and loads can be defined.

The PV and the ESS are interfaced to the grid through a DC/DC boost converter and a bi-directional buck-boost DC/DC converter, respectively. The primary source of power generation for the DC microgrid is the PV, which is controlled to operate at both current-mode control (CMC) and voltage-mode control (VMC). The ESS is

utilized to compensate the mismatch between generation and consumption in the islanded mode of the microgrid. The microgrid can be isolated by a DC circuit breaker (CB).
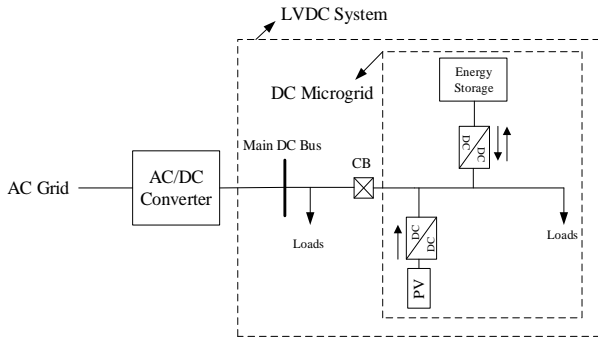


**Fig. 1.** The layout of the investigated LVDC system

### 2.2. Grid operating modes

Different operating modes are considered for the LVDC system, which are summarized in Table 1. In column 5, $P_{PV}$ is the PV maximum power and $P_{load}$ is the load power.

In mode 1, the LVDC system is connected to the grid and the DC bus voltage is controlled by VSC. The PV and the ESS are in off-state. In operating modes 2-5, the PV is working in CMC before the fault occurrence (pre-fault). After the fault clearance (post-fault), the state of the PV depends on the ESS state and the operating condition. In mode 2, the ESS is in off-state and the PV power is less than the load power. Therefore, to prevent the voltage instability because of the generation-load mismatch, the PV post-fault state is off. In modes 3 and 4, the PV maximum power is larger than the load power. In the islanded DC microgrid, The PV is going to work in VMC to provide the required power of the load and to regulate the DC voltage. In mode 4 compared to mode 3, the ESS is in on-state and is switched to mitigate the fault transients. Mode 5 refers to the case where the PV remains in CMC for post-fault condition. A switching logic is proposed to be used for the ESS to mitigate the fault transients in short-term application and to balance insufficient/surplus power in long-term application.

## 3. SYSTEM MODELING AND CONTROL

### 3.1. Modeling of PV system

Fig. 2 shows a PV array which is connected to the LVDC system through a DC/DC boost converter. Modeling of PV arrays and the control algorithm of the converter depend on the duration of the study. For long-term studies, especially in the field of the operation and control of the AC/DC microgrids, a detailed model of PV arrays is proposed which considers the ambient temperature and solar radiation. In the grid connected mode, a maximum power point tracking (MPPT) algorithm is utilized in the

converter to deliver the maximum available power to the grid. In islanded mode, the converter works in voltage-mode control to support the balance of power and regulate the DC voltage [40-41].

The PV arrays are modeled as a constant DC voltage source interfaced with the grid through a power-electronic converter in the literature which studies the protection of the microgrids and power quality issues. Fast control algorithms are implemented to the converter to regulate current and voltage in grid connected and islanded mode of operation so that the PV system acts like a constant power source. This assumption is possible because the system is studied during the fault transient which is fractions of a second. In this short period of time, the ambient temperature and solar radiation is almost constant [42-46].

This paper considers the PV array as a constant voltage source because of very fast transients of the DC faults. Also, fast current and voltage mode control algorithms are applied to the DC/DC boost converter. The converter is switched between two control modes according to the operating modes. Status of the isolating circuit breaker is applied as an input signal to switch the PV from the pre-fault state to the post-fault state.
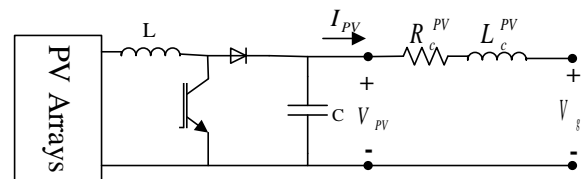


**Fig. 2.** A boost DC/DC converter connected to the PV arrays

**Table 1.** LVDC system operating modes

| Mode | PV pre-fault state | PV post-fault state | ESS state | Operating condition |
|------|-------------------|--------------------|-----------|---------------------|
| 1 | off | off | off | $P_{PV}=0$ |
| 2 | CMC | off | off | $P_{PV}<P_{load}$ |
| 3 | CMC | VMC | off | $P_{PV}>P_{load}$ |
| 4 | CMC | VMC | on | $P_{PV}>P_{load}$ |
| 5 | CMC | CMC | on | a)  $P_{PV}<P_{load}$ b)  $P_{PV}>P_{load}$ |

### 3.1.1. Control algorithm of the PV system

A boost DC/DC converter is used to connect the PV to the LVDC system. According to the operating modes of the grid discussed in the Section 2.2, the PV system should operate in both current and voltage control modes. The block diagram of the proposed control modes for the PV system is shown in Fig. 3. In current-mode control, the injected current of the PV is measured and is compared with its reference value. The error signal is applied to the PI controller and PWM block generates the

gate pulses according to the output of the PI block. In voltage-mode control, the reference value of the PV voltage is calculated by using Eq. (1), and then is compared with the PV measured voltage. The Saturation block imposes upper and lower bounds on the error signal.

$$V_{PV}^{ref} = V_g^{ref} + 2R_c^{PV}I_{PV} + 2L_c^{PV}\frac{dI_{PV}}{dt} \quad (1)$$

Where, $V_{PV}^{ref}$ is the PV reference voltage, $V_g^{ref}$ is the grid reference voltage, $I_{PV}$ is the PV current and $R_c^{PV}$ and $L_c^{PV}$ are the PV cable resistance and inductance, respectively.
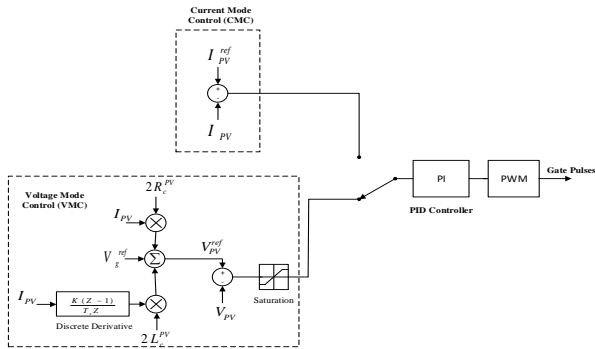


**Fig. 3.** The control system of PV

### 3.2. Modeling of ESS
The authors of the current study assume the ESS as a constant DC voltage source which is connected to the DC grid through a bi-directional DC/DC converter as shown in Fig. 4. A control system similar to the voltage-mode control of the PV converter regulates the output voltage of the ESS. The ESS can operate in both charging and discharging modes regarding the grid operating conditions.
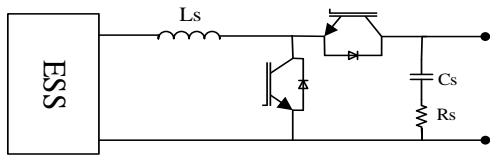


**Fig. 4.** Bi-directional converter connected to the ESS

### 3.3. Load Modeling
A combination of resistive and constant power loads (CPL) are considered as the load model in this paper as shown in Fig. 5. Constant power load is modeled by a resistive load, which is connected to the DC bus through a tightly regulated buck converter, an input filter, and a diode. The regulator provides specified voltage and current to the load regardless of voltage disturbances on the bus; therefore, the regulator appears as a load that draws constant power from the bus. The input filter prevents the switching ripple of the converter from going to the DC bus. The diode is needed to prevent reverse current from the load to the system in regenerative mode of the load.

The resistive load at the output of the buck converter is given by

$$R_{load} = \frac{(V_{out})^2}{P_{const}} \quad (2)$$

Where, $V_{out}$ is the output voltage of the regulator and $P_{const}$ is the constant power of the load.
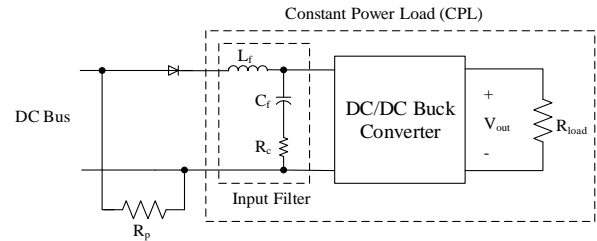


**Fig. 5.** The load model

## 4. CASE STUDIES AND SIMULATION RESULTS
In this section, the behavior of the LVDC system is studied under the fault conditions through the simulations using MATLAB software. The schematic diagram of the simulated LVDC system is shown in Fig. 6. The system has radial structure and is connected to the AC network through a controlled rectifier, which is grounded solidly as shown in Fig. 7. The output of the rectifier is connected to the main DC bus which feeds other three consumer buses. The PV and the ESS can be connected to buses 2 and 3, respectively. The system parameters are listed in Table 2.
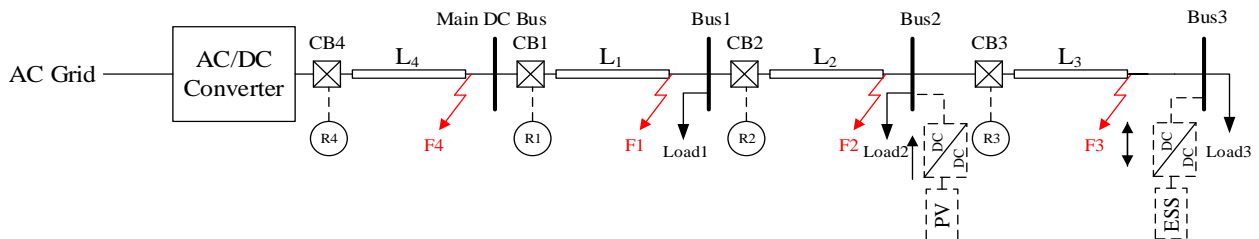


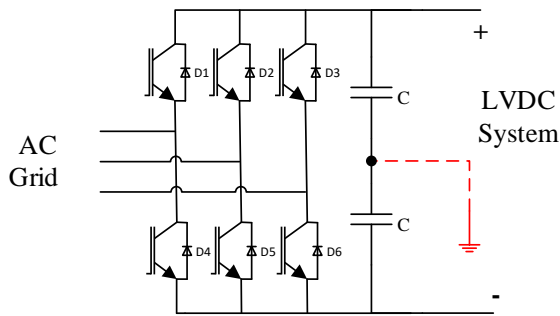**Fig. 6.** Schematic diagram of the simulated LVDC system

**Fig. 7.** Model of the controlled rectifier

**Table 2.** LVDC system parameters

| AC/DC Converter | Input AC voltage= 240V, 60 Hz , Output DC voltage=400 V   Power=50kVA   C=75 mF |
|---|---|
| DC Cables | $R_L$=0.121Ω/km, $L_L$=0.34mH/km |
| | L1                    Length=300 m |
| | L2                    Length=500 m |
| | L3                    Length=500 m |
| | L4                    Length=10 m |
| DC load | Input filter: $L_f$= 0.2 µH,  $C_f$=225 µF,  $R_c$=0.05 Ω |
| | Constant power= 8 KW |
| | Constant Resistance= 20 Ω |
| PV system converter | L=5 mH    C= 3 mF   $R_c^{PV}$=0.5 Ω    $L_c^{PV}$ =0.1 mH |
| | Switching Frequency=10 KHz |
| ESS converter | Ls=5 mH   Cs=10 mF        Rs=0.2 Ω |
| | Switching Frequency=10 KHz |

The protective devices installed on the system are ultra-high speed circuit breakers and overcurrent relays. Faults F1-F4 are placed at the end of the lines of the system and the system behavior is studied for the grid operating modes presented in Table 1. The following assumptions have been made in the analysis.

1) Only pole-to-ground faults are considered, since they have a higher probability of occurrence.
2) Effects of the loads on the fault currents are neglected: The standard IEC 60909 suggests to obtain fault current results for an unloaded network. The most short-circuit studies ignore the load current since the magnitude of the fault current is extremely greater than the load current. On the other hand, the loads considered here are combination of resistive and constant power loads. The resistive loads (passive components) don't affect the fault current. In the CPL model, as described earlier, there is a diode on the input DC bus of the load to prevent reverse current feed to a line-side fault.
3) The permissible minimum and maximum values of the buses voltage are assumed to be 300V and 600V, respectively.
4) The PV current can be increased to 2.5 times its nominal current during the faults.

### 4.1. Case 1

In this case, the PV and the ESS are not connected to the system. Faults F1-F4 are placed in the system and the faults currents passed through the lines are measured. The logic of Inverse Definite Minimum Time (IDMT) relay can be used to set overcurrent relays. The pickup value of current, operating time and discrimination margin must be determined.

The overcurrent relays should distinguish between the normal operating condition and the faulty condition of the system. Pickup currents of the relays are chosen as a coefficient of full load steady state currents flowing through the respective lines to avoid the relays operation for normal operating conditions. Therefore, to determine pickup values, a current coefficient is defined as follows:

$$N_i = {I_{mLi}}/{I_{sLi}} \tag{3}$$

Where, $I_{mLi}$ is the maximum fault current passing through ith line and $I_{sLi}$ is the full load steady state current which is chosen based on the maximum operation current expected to be passed through ith line. The obtained current coefficients for the considered faults and the full load steady sate currents are shown in Table 3.

According to the values shown with red color, the overcurrent relays can be set on 6 times the full load steady state currents of the respective lines to have a selective protection. However, the current passed through the line 4 for F4 reaches 93 times its steady state value. This fault current can damage the converter and its output capacitors. To solve this problem, the midpoint of the output capacitors is grounded by 0.1 ohm resistor. The faults F1-F4 are applied again to the system and results are listed in Table 4. By changing the grounding method of the system, the current coefficient of the line 4, N4, is reduced from 93 to 8.35. Consequently, the possibility of damage to the converter and output capacitors is reduced. The set point of the IDMT overcurrent relays can be chosen 5 times the full load steady state current. Therefore, the pickup currents of the relays R1-R4 are 750 A, 500 A, 250 A, and 1250 A, respectively. The fault current reaches its maximum value after 2 ms. Therefore, the operating time is chosen 2 ms and the discrimination margin is chosen 1 ms.

**Table 3.** Current coefficients of the faults for solidly grounded system

| Fault | $I_{sL1}$ | $I_{sL2}$ | $I_{sL3}$ | $I_{sL4}$ | N1 | N2 | N3 | N4 |
|---|---|---|---|---|---|---|---|---|
| F1 | 150 | 100 | 50 | 250 | **11.02** | - | - | 6.97 |
| F2 | 150 | 100 | 50 | 250 | 4.77 | **6.67** | - | 2.86 |
| F3 | 150 | 100 | 50 | 250 | 3.07 | 4.28 | **7.64** | 1.84 |
| F4 | 150 | 100 | 50 | 250 | - | - | - | **93** |

**Table 4.** Current coefficients of the faults for the system grounded by resistor

| Fault | $I_{sL1}$ | $I_{sL2}$ | $I_{sL3}$ | $I_{sL4}$ | N1 | N2 | N3 | N4 |
|-------|-----------|-----------|-----------|-----------|-----|------|-----|------|
| F1 | 150 | 100 | 50 | 250 | **7.5** | - | - | 4.88 |
| F2 | 150 | 100 | 50 | 250 | 4.1 | **5.65** | - | 2.46 |
| F3 | 150 | 100 | 50 | 250 | 2.95 | 4.03 | **7.6** | 1.77 |
| F4 | 150 | 100 | 50 | 250 | - | - | - | **8.35** |

Also, high speed fuses and high technology circuit breakers are needed for the protection of the system. Solid-state circuit breakers (SSCBs) are the fastest type of DC circuit breakers (DCCBs) that can operate in less than 1ms [47]–[49]. This type of DCCBs is considered in the paper.

## 4.2. Case 2

To study effects of the distributed generations on the system protection, a PV unit is connected to bus 2 through a current controlled DC/DC boost converter as shown in Fig. 8. The nominal injected current of the PV is increased and the operation of the protective relays is studied. Firstly, the injected current of the PV is considered as 25 A, half of the consumer current in bus 2. As seen in Table 5, for F2 and F3, the current coefficients N2 and N3 are 5.34 and 7.94, respectively. These values are greater than the setting values of the relays, which make them operate correctly. Compared to the N2 and N3 values listed in Table 4, it becomes clear that the PV decreases the amount of the fault current in the upstream line (line 2) and increases it in the downstream line (line 3). In fact, supplying part of the load power by the PV injected power decreases the steady state current in the upstream lines which leads to decrease in the amplitude of the fault current. As listed in Table 5, the N2 value is decreased for further increase in the PV injected current and reaches 4.98 when the PV current equals to 80 A. In this condition, the relay on line 2 (R2) is unable to detect F2. Therefore, the protective relays may be affected and cannot operate correctly for large injected current of the PV. In this paper, the authors try to solve this problem with minimum changes in the system protection and focus mainly on the setting of the O.C relays. It is proposed to add relays R12, R22, and R32 with the backward directions to the end of the lines as

shown in Fig. 8.

**Table 5.** Current coefficients of the faults in the presence of the PV

| Fault | Ispv (A) | Npv | N2 | N3 |
|-------|----------|------|--------|--------|
| F2 | 25 | 5.6 | **5.34** | - |
| F3 | 25 | 2.32 | 3.85 | **7.94** |
| F2 | 60 | - | 5.03 | - |
| F2 | 75 | - | 5.028 | - |
| F2 | 80 | - | 4.98 | - |

The forward and backward relays should coordinate with their downstream relays, respectively. For example, R1 should be the backup protection of R2. In case of R2 does not trip instantaneously, R1 should trip after a delay time which is defined as the discrimination margin in the setting of the O.C relays. Also, the pickup currents of the forward relays must be changed according to the changes in the fault currents which depend on the PV maximum output power. The pickup currents of the backward relays are determined by locating faults at the beginning of the lines. As shown in Table 5, the pickup current of R2 can be chosen 4 times the full load steady state current of line 2. The operating time for the pickup values is chosen 2ms for all relays. The discrimination margin is chosen 1ms to have selective protection between relays which are in the same direction. More advanced protection strategies such as differential and smart protection can also be used in order to allow the PV penetration. However, the change of the whole distribution protection is very expensive and perhaps unrealistic idea. An issue for overcurrent and directional based protections is high resistive fault detection. In the case of high resistive faults, the direction of the current may not be changed which makes the directional protection blind. Currently, in terms of fast speed requirements and high resistive DC fault detection, differential protection is the promising solution compared to other methods. The challenge with differential protection is the cost where advanced communication and synchronizing devices are required. After isolating the faulty section, to refuse the power outage for the downstream consumers, the healthy section of the system can be operated independently as a micro-grid.
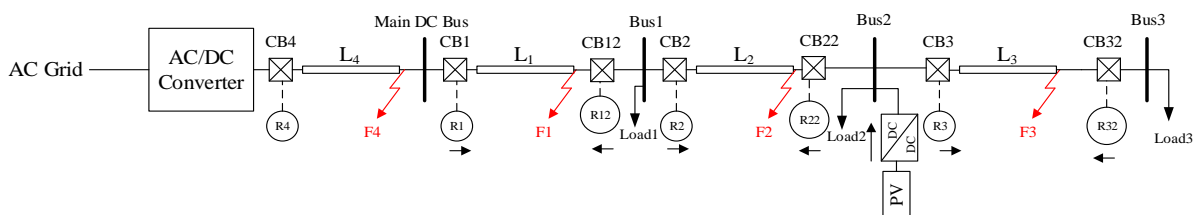


**Fig. 8.** Schematic diagram of the protection arrangement for case 2

Providing the required power of the consumers and keeping the voltage stability are the main conditions for the healthy part of the system to work as a microgrid. Otherwise, undervoltage or overvoltage relays will detect the voltage instability and the loads will be isolated from the system by the protective devices.

In the next cases, a pole-to-ground fault is placed in the middle of the line 2 at 0.3 s and the system behavior is studied. The faulty section is isolated at 0.301 s by high-speed circuit breakers. Buses 2 and 3 can be operated as a DC microgrid.

### 4.3. Case 3

In this case, the injected current of the PV is assumed to be 100 A and after isolating the faulty section, the PV is operated in voltage-mode control. The energy storage is not in the system. The simulation results are represented in Figs 9 and 10.

As shown in Fig. 9, the PV works in current-mode control before the fault occurrence and injects 100 A to the network. In the fault condition, the PV current reaches 188 A at 0.301 s before the operation of the system protection. According to the permissible limit of the PV current, the PV will be in the network during the fault and its protection will not act for this current value. After isolating the faulty section, the fault current decreases and the PV control mode is changed to VMC at 0.302 s. In the voltage-mode control, the PV supplies 84 A for the microgrid consumers.

The voltage profiles of the buses, $V_{b1}$ to $V_{b3}$, are shown in Fig. 10. The voltage of bus 1 drops to 310 V during the fault and rises to 550 V after the fault clearance. These voltage variations are in the permissible limit, and therefore the undervoltage and overvoltage relays in bus 1 do not act for these voltage levels. $V_{b2}$ and $V_{b3}$ vary from 265 V to 408 V and from 256 V to 407 V, respectively. The voltage drop in both buses exceeds the lower permissible limit of the voltage (300 V). Subsequently, it leads to the operation of the undervoltage relays and outage of the loads in the corresponding buses. Therefore, the DC microgrid cannot work in the islanded mode. Keeping the voltage variation in the permissible limits for the healthy buses of the system is necessary to have a correct protection. To solve this challenge, it is proposed to add an ESS to the system which its performance is studied in case 4.

### 4.4. Case 4

The injected current of the PV is 100 A and after isolating the faulty section, the PV is operated in the voltage-mode control. The energy storage is connected to bus 3 through a controlled switch as shown in Fig. 11.

Status of the switch (on or off) is controlled by a switching logic. To mitigate the transient disturbances of the voltage in case 3, a switching logic based on the voltage variations is chosen. This logic is named transient state switching logic. If the voltage variations are in the permissible limit, the switch is in off-state. Otherwise, it is in on-state to limit the voltage oscillations in the healthy buses, and then to refuse the operation of the voltage protection. The permissible limit of the bus 3 voltage for the storage switching is selected from 360 V to 420 V.

As shown in Fig. 12, the PV current reaches 165 A during the fault and it is less than its value in case 3. The voltage profiles of the buses, $V_{b1}$ to $V_{b3}$, are shown in Fig. 13. Variations of bus 1 voltage are between 318 V and 545 V, which is close to its variations in case 3. This is because of the far distance between the energy storage and bus 1 which makes its effect inconspicuous on bus 1. $V_{b2}$ and $V_{b3}$ vary from 303 V to 407 V and from 321 V to 405 V, respectively. Compared to the case 3, the voltage variations are limited and the buses voltages are above 300 V. Therefore, undervoltage relays on buses 2 and 3 don't act and the loads don't have any outage. As shown in Fig. 14, the energy storage helps to limit voltage oscillations in the fault condition by injecting or absorbing current, positive or negative currents, in undervoltage and overvoltage conditions, respectively.

### 4.5. Case 5

The PV is operated in the current-mode control and remains in this mode after isolating the faulty section. Therefore, the energy storage is needed to stabilize the voltage during the fault and after its clearance when the healthy part of the system is operated as a microgrid.
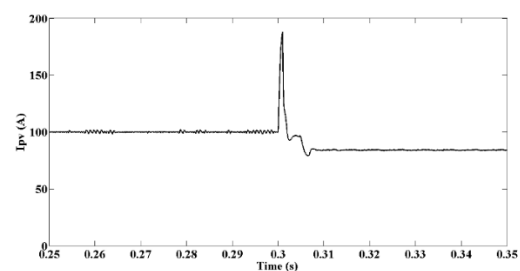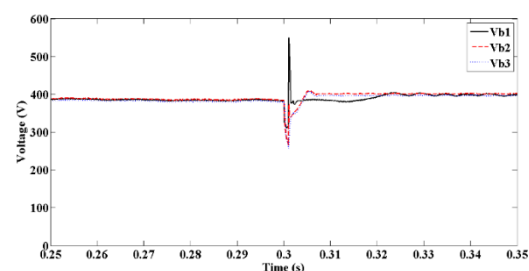


**Fig. 9.** PV injected current (case 3)



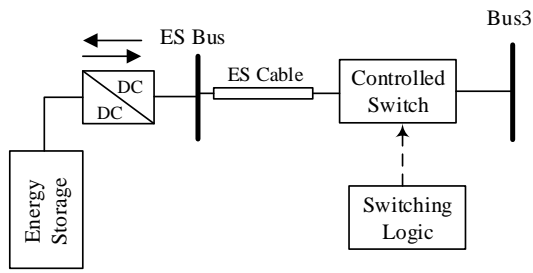**Fig. 10.** The voltage profiles (case 3)

**Fig. 11.** The energy storage connection to the bus 3
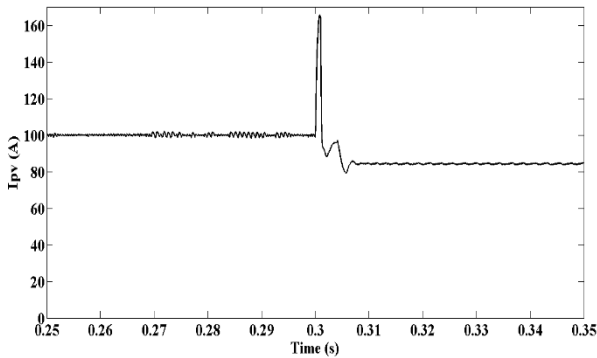


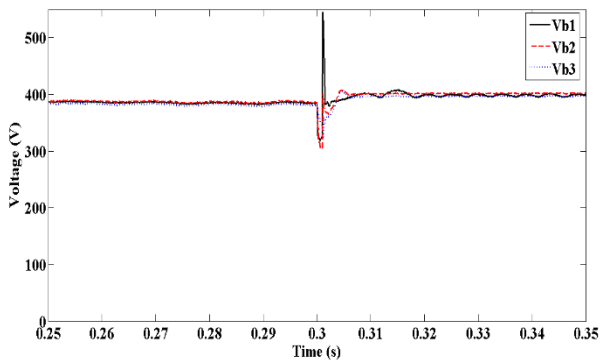**Fig. 12.** PV injected current (case 4)



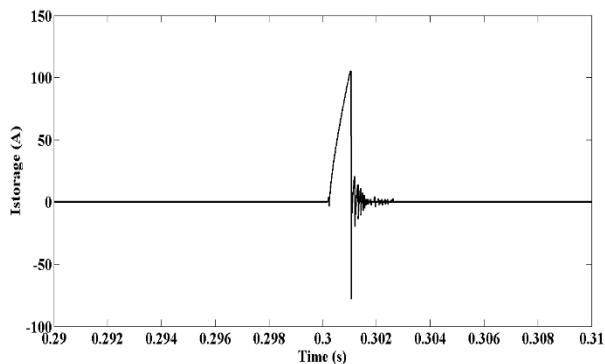**Fig. 13.** The voltage profiles (case 4)



**Fig. 14.** ESS injected current (case 4)

### 4.5.1. Using the transient state switching logic

Firstly, the transient state switching logic is applied to ESS switch similar to case 4. As shown in Figs 15 and 16, the bus 3 voltage has continuing oscillations and the energy storage is switched continuously because of the unbalance between the PV injected power and the load

power. Therefore, a new switching logic is needed to be designed for this case.

After isolating the faulty section, the injected current of the PV which is controlled by the controller may be greater than or less than the required current of the loads in the healthy part of the system. Therefore, the switching logic of the storage should detect the unbalance between the generation and the consumption and enters the energy storage to absorb the surplus power either to inject the required power. The storage remains in the system until the unbalance exists. Measuring the PV power and comparing it with the load power can be useful. However, it does not seem logical for a system with multiple PV units. The following logic is proposed to detect the unbalance between the generation and the consumption.
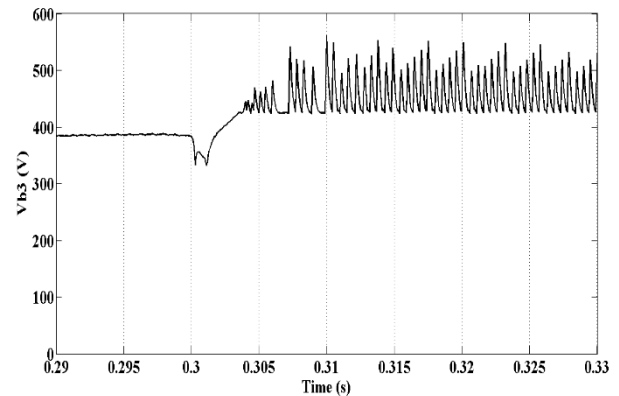


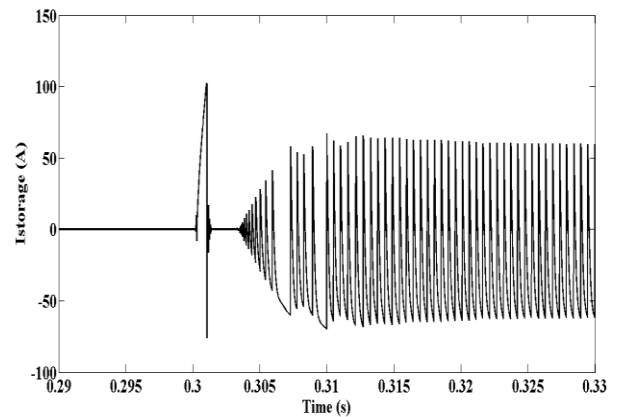**Fig. 15.** The bus 3 voltage under the transient state switching logic of ESS (case 5)



**Fig. 16.** The storage injected current under the transient state switching logic (case 5)

### 4.5.2. The proposed switching logic

The bus 3 voltage is measured continuously and is compared with the standard range. A switching sequence is proposed in (4) for the storage switch to distinguish the transient state (the voltage instability because of the fault) from the steady state (the voltage instability because of

the unbalance between the generation and the consumption). If the fault is the only cause of the voltage instability, the voltage, after isolating the fault current in a short period of time, returns inside its standard range, and therefore the energy storage system doesn't need to remain in the network. However, in the case that there is an unbalance between generation and consumption, the energy storage must remain connected to the grid to overcome the unbalance condition and to keep the voltage in the standard range. A successive closing and opening operations are proposed to determine whether the ESS must remain connected to the grid or be disconnected after a short period of time.

$$C\text{-}1ms\text{-}OC\text{-}1ms\text{-}OC \qquad\qquad (4)$$

Where, C indicates closing operation of the switch. The switch closes when the measured voltage exceeds the standard range. OC represents opening operation immediately followed by a closing operation without any intentional time delay. 1 ms is the time interval between two operations.

After the second opening operation, if the measured voltage still doesn't meet the standard range, the unbalance condition is detected. The switch closes for the third time and remains in that position. The energy storage compensates the difference between the generation and the consumption and stabilizes the voltage.

The block diagram of the proposed logic is shown in Fig. 17. The performance of the proposed logic is proved for Ipv=70 A when the generation is less than the consumption (heavy load condition) and for Ipv=100 A when the generation is greater than the consumption (light load condition).
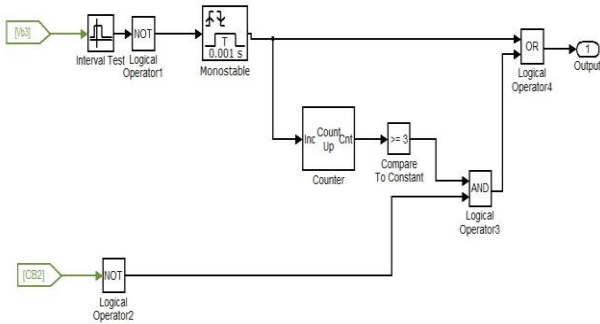


Fig. 17. The proposed switching logic for ESS

**Heavy load condition:**

The simulation results for Ipv=70 A are shown in Figs 18-21. The injected current of PV reaches 140 A during the fault. The storage is switched according to the proposed logic and remains connected to the system after the third closing operation. The storage injects 14 A to

the system to compensate the power unbalance. $V_{b1}$ and $V_{b2}$ vary from 327.5 V to 595.5 V and from 306 V to 446.5 V, respectively. The bus 3 voltage drops to 345 V during the fault.

**Light load condition:**

The simulation results for Ipv=100 A are shown in Figs 22-25. The injected current of the PV reaches 163 A during the fault. The storage is switched according to the proposed logic and remains connected to the system after the third closing operation. The storage absorbs 16 A from the system to provide the power balance. $V_{b1}$, $V_{b2}$ and $V_{b3}$ are between 314.6 V-536 V, 301 V-462 V and 323.5 V-420.5 V, respectively. According to the simulation results, the proposed switching logic has a good performance in both light and heavy load conditions. Furthermore, it lets the DC microgrid work in islanded mode by keeping the voltage in the standard range during the fault transients and by injecting/absorbing the required/surplus power during the power unbalance condition.
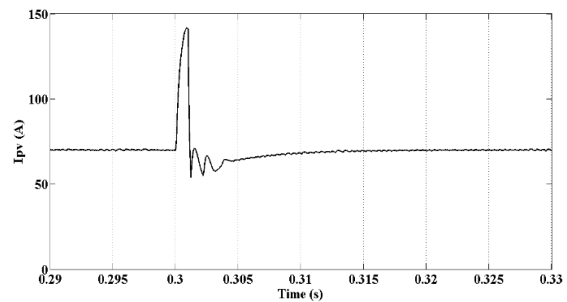


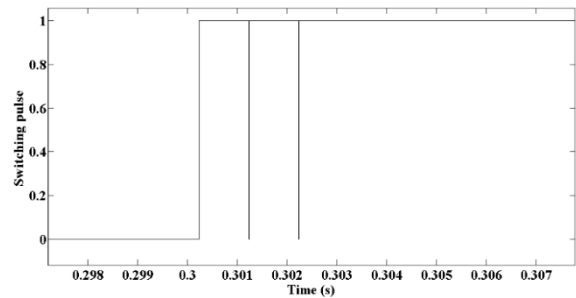Fig. 18. PV injected current under the proposed switching logic (Ipv=70 A)

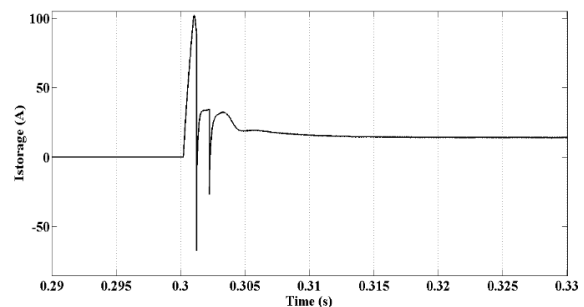

Fig. 19. The switching pulse of the ESS switch (Ipv=70 A)



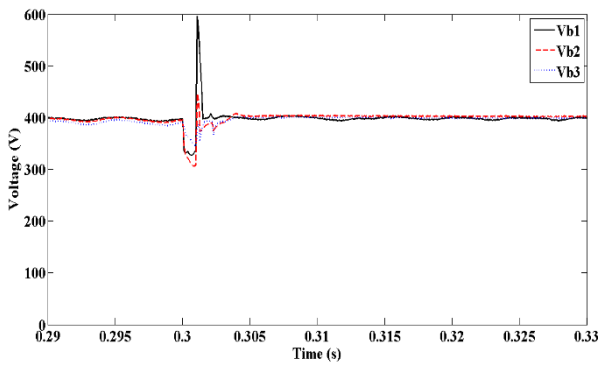Fig. 20. ESS injected current under the proposed switching logic (Ipv=70 A)

**Fig. 21.** The voltage profiles (Ipv=70 A)



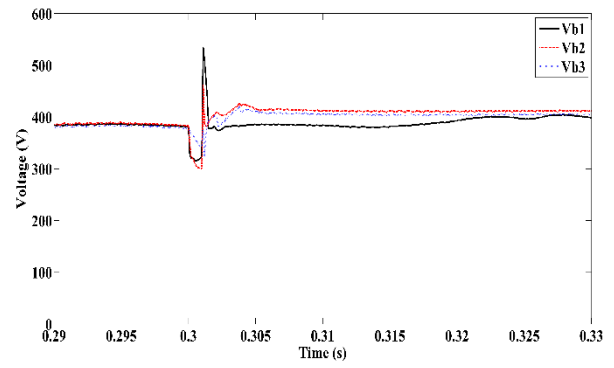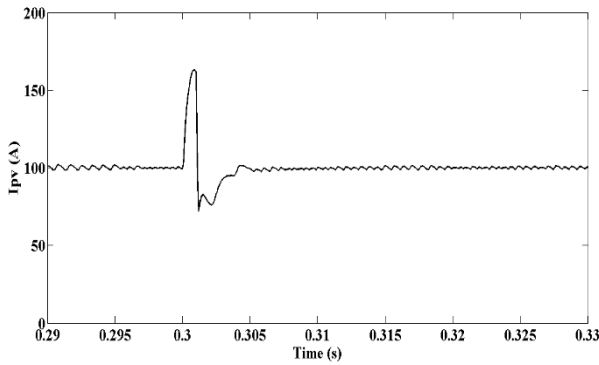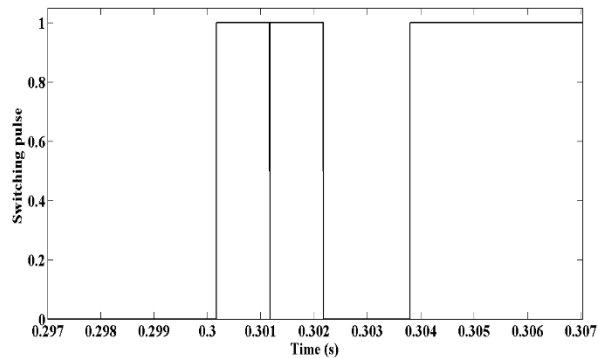**Fig. 22.** PV injected current under the proposed switching logic (Ipv=100 A)



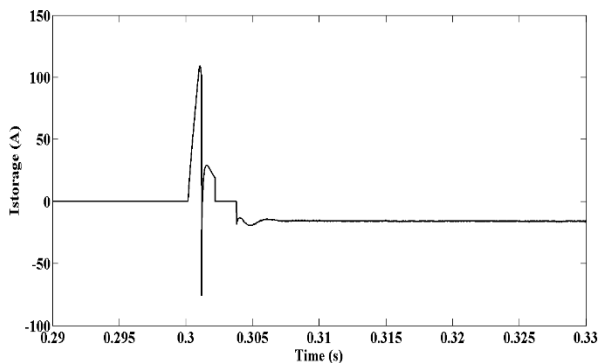**Fig. 23.** The switching pulse of the ESS switch (Ipv=100 A)



**Fig. 24.** ESS injected current under the proposed switching logic (Ipv=100 A)



**Fig. 25.** The voltage profiles (Ipv=100 A)

## 5.   COMPARISON OF RESULTS

Firstly, a radial low voltage DC distribution system is modeled in case 1 and overcurrent based protection is discussed. Results show that the system can be protected by choosing a suitable grounding method and applying high speed breaking devices.

Then, in case 2, a PV unit is added to case 1 and its effect on the system protection is analyzed. In comparison to case 1, the introduction of the PV to the system changes the fault currents of the upstream and downstream lines. Therefore, it leads to malfunctions in the relays operations, especially for large powers of the PV. Directional overcurrent protection is proposed to solve this problem. Also, the DC microgrid cannot operate after isolating the faulty section because the PV power is lower than the load power.

In case 3, the demanded power is less than the maximum power of the PV. Therefore, after isolating the faulty section, the PV is operated in voltage-mode control to provide the required power of the load. However, the PV cannot keep voltages of the healthy buses inside the standard level. Subsequently, it leads to the operation of the undervoltage relays and outage of the loads. In the islanded mode of operation, the DC microgrid voltage must be controlled and the power of the loads must be met.

To solve the problem of case 3, an energy storage system is added to the system in case 4. A switching logic named "transient state switching logic" is defined for the ESS. It has good performance in mitigating the voltage oscillations of the DC microgrid. In fact, in islanded mode operation of the DC microgrid, the PV supplies the demanded power of the load and the ESS controls the voltage level.

In case 5, the PV is operated in current-mode control for post-fault state and its output power will be lower or larger than the load power. Therefore, in order to operate

the DC microgrid in islanded mode and to refuse protective relays malfunction, the ESS must compensate the mismatch between the PV power and the load power and simultaneously it must control the voltage level. To do this, a new switching logic based on successive opening and closing operations is proposed for the ESS and its performance is verified using simulation. As a result, control modes of the PV and switching mechanisms of the ESS affect the protection of the DC microgrid and they must be designed correctly to refuse unwanted outages of the system.

## 6.  CONCLUSIONS

This paper studies the protection of the low voltage DC grid in the presence of the distributed generation. By Integrating the PV unit and the energy storage system to the LVDC system, part of the system can be operated as a DC microgrid. The microgrid goes to islanded mode when there is a fault in the main system. Changing the structure of the LVDC system introduces new protection challenges to the system. Therefore, different operating modes of the system are classified depending on the PV, the ESS and the load conditions. The system simulation has been carried out using MATLAB software to analyze all cases. The results show the effects of the system operating modes on its protection. Control methods of the PV, switching mechanisms of the ESS and loading condition of the system are the main factors which result in the new challenges in the DC microgrid protection. Some methods have been proposed to solve these challenges. The methods are generally based on the changing the protection arrangement, the grounding method and the switching logic of the energy storage system. Finally, the proposed methods are validated through simulation.

### REFERENCES

[1]  A. T. Elsayed, A. A. Mohamed, and O. A. Mohammed, "DC microgrids and distribution systems: An overview," *Electr. Power Syst. Res.*, vol. 119, pp. 407-417, 2015.

[2]  M. E. Baran and N. R. Mahajan, "DC distribution for industrial systems: opportunities and challenges," *IEEE Trans. Ind. Appl.*, vol. 39, no. 6, pp. 1596-1601, 2003.

[3]  M. Brenna, G. C. Lazaroiu, G. Superti-Furga, and E. Tironi, "Bidirectional front end converter for DG with disturbance insensitivity and islanding-detection capability," *IEEE Trans. Power Deliv.*, vol. 23, no. 2, pp. 907-914, 2008.

[4]  D. Georgakis, S. Papathanassiou, N. Hatziargyriou, A. Engler, and C. Hardt, "Operation of a prototype microgrid system based on micro-sources quipped with fast-acting power electronics interfaces," Proce. *IEEE 35th Annu. Power Electron. Specialists Conf.*, 2004, pp. 2521-2526.

[5]  K. Mizuguchi, S. Muroyama, Y. Kuwata, and Y. Ohashi, "A new decentralized DC power system for telecommunications systems," Proce. *12th Int. Conf.*

[6]  D. Salomonsson and A. Sannino, "Low-voltage DC distribution system for commercial power systems with sensitive electronic loads," *IEEE Trans. Power Deliv.*, vol. 22, no. 3, pp. 1620-1627, 2007.

[7]  Y.-S. Oh, J. Han, G.-H. Gwon, D.-U. Kim, and C.-H. Kim, "Development of fault detector for series arc fault in low voltage DC distribution system using wavelet singular value decomposition and state diagram," *J. Electr. Eng. Technol.*, vol. 10, no. 3, pp. 766-776, 2015.

[8]  D. Hur and R. Baldick, "An economic analysis of potential cost savings from the use of low voltage DC (LVDC) distribution network," *J. Electr. Eng. Technol.*, vol. 9, no. 3, pp. 812-819, 2014.

[9]  D. Afamefuna, I.-Y. Chung, D. Hur, J.-Y. Kim, and J. Cho, "A techno-economic feasibility analysis on LVDC distribution system for rural electrification in south korea," *J. Electr. Eng. Technol.*, vol. 9, no. 5, pp. 1501-1510, 2014.

[10]  G. Byeon, C.S. Hwang, J.H. Jeon, S.K. Kim, J.Y. Kim, Kim, K., B. Ko and E.S. Kim, "Complementary power control of the bipolar-type low voltage DC distribution system," *J. Electr. Eng. Technol.*, vol. 10, no. 3, pp. 786-794, 2015.

[11]  W. Jewell and Zhouxing Hu, "The role of energy storage in transmission and distribution efficiency," Proce. *IEEE PES T&D Conf. Exposition*, 2012, pp. 1-4.

[12]  D. Manz, R. Piwko, and N. Miller, "Look before you leap: the role of energy storage in the grid," *IEEE Power Energy Mag.*, vol. 10, no. 4, pp. 75-84, 2012.

[13]  Q. Jiang and H. Wang, "Two-time-scale coordination control for a battery energy storage system to mitigate wind power fluctuations," *IEEE Trans. Energy Convers.*, vol. 28, no. 1, pp. 52-61, 2013.

[14]  B. P. Roberts and C. Sandberg, "The role of energy storage in development of smart grids," *Proc. IEEE*, vol. 99, no. 6, pp. 1139-1144, Jun. 2011.

[15]  A. Hatefi einaddin, A. Sadeghi Yazdankhah, and R. Kazemzadeh, "Power management in a utility connected micro-grid with multiple renewable energy sources," *J. Oper. Autom. Power Eng.*, vol. 5, no. 1, pp. 1-10, Jun. 2017.

[16]  H. Shayeghi and E. Shahryari, "Optimal operation management of grid-connected microgrid using multi-objective group search optimization algorithm," *J. Oper. Autom. Power Eng.*, vol. 5, no. 2, pp. 227-239, Dec. 2017.

[17]  R. Tiwari and M. Anantha Kumar, "Integration and distribution of renewable sources in DC micro grid with energy storage system," *Int. J. Innov. Res. Sci. Eng. Technol.*, vol. 3, no. 3, 2014.

[18]  L. K. Letting, J. L. Munda, and Y. Hamam, "Dynamic performance analysis of an integrated wind-photovoltaic microgrid with storage," *Int. J. Smart Grid Clean Energy*, vol. 3, no. 3, 2014.

[19]  K. Strunz, E. Abbasi, and D. N. Huu, "DC microgrid for wind and solar power integration," *IEEE J. Emerg. Sel. Top. Power Electron.*, vol. 2, no. 1, pp. 115-126, Mar. 2014.

[20]  K. H. (M. Tech), "Battery energy management system for DC micro grids with fuzzy controller," *Int. J. Innov. Res. Sci. Eng. Technol.*, vol. 3, no. 1, pp. 1486-1493, Jan. 1970.

[21]  B. Liu, F. Zhuo, Y. Zhu, and H. Yi, "System operation and energy management of a renewable energy-based DC micro-grid for high penetration depth application," *IEEE Trans. Smart Grid*, vol. 6, no. 3, pp. 1147-1155, May 2015.

[22]  J.Y. Kim J.H. Jeon, S.K. Kim, C. Cho, J.H. Park, H.M.

Kim, K.Y. Nam, "Cooperative control strategy of energy storage system and microsources for stabilizing the microgrid during islanded operation," *IEEE Trans. Power Electron.*, vol. 25, no. 12, pp. 3037-3048, Dec. 2010.

[23] Y. Zhang, H.Jie Jia, and L. Guo, "Energy management strategy of islanded microgrid based on power flow control," Proce. *IEEE PES Innovative Smart Grid Technol.*, 2012, pp. 1-8.

[24] D. Shen, A. Izadian, and P. Liao, "A hybrid wind-solar-storage energy generation system configuration and control," Proce. *IEEE Energy Convers. Congr. Exposition*, 2014, pp. 436-442.

[25] K. Rouzbehi, A. Miranian, J. I. Candela, A. Luna, and P. Rodriguez, "intelligent voltage control in a DC micro-grid containing PV generation and energy storage," Proce. *IEEE PES T&D Conf. Exposition*, 2014, pp. 1-5.

[26] A. Hooshyar and R. Iravani, "Microgrid protection," *Proc. IEEE*, vol. 105, no. 7, pp. 1332-1353, 2017.

[27] J. Yang, J. E. Fletcher, and J. O'Reilly, "Multiterminal DC wind farm collection grid internal fault analysis and protection design," *IEEE Trans. Power Deliv.*, vol. 25, no. 4, pp. 2308-2318, 2010.

[28] J. Yang, J. E. Fletcher, and J. O'Reilly, "Short-circuit and ground fault analyses and location in VSC-based DC network cables," *IEEE Trans. Ind. Electron.*, vol. 59, no. 10, pp. 3827-3837, 2012.

[29] J. Candelaria and J.-D. Park, "VSC-HVDC system protection: A review of current methods," Proce. *IEEE PES Power Syst. Conf. Exposition*, 2011, pp. 1-7.

[30] M. K. Bucher, M. M. Walter, M. Pfeiffer, and C. M. Franck, "Options for ground fault clearance in HVDC offshore networks," Proce. *IEEE Energy Convers. Congr. Exposition*, 2012, pp. 2880-2887.

[31] P. Kundur, N. J. Balu, and M. G. Lauby, Power system stability and control. McGraw-Hill, 1994.

[32] R. K. Mallick and R. K. Patnaik, "Fault analysis of voltage-source converter based multi-terminal HVDC transmission links," Proce. *Int. Conf. Energy Autom. Signal*, 2011, pp. 1-7.

[33] J. Yang, J. Zheng, G. Tang, and Z. He, "Characteristics and recovery performance of VSC-HVDC DC transmission line fault," Proce. *Asia-Pacific Power Energy Eng. Conf.*, 2010, pp. 1-4.

[34] M. E. Baran and N. R. Mahajan, "Overcurrent Protection on voltage-source-converter-based multiterminal DC distribution systems," *IEEE Trans. Power Deliv.*, vol. 22, no. 1, pp. 406-412, 2007.

[35] S. R. B. Vanteddu, A. Mohamed, and O. Mohammed, "Protection design and coordination of DC distributed power systems architectures," Proce. *IEEE Power Energy Soc. Gen. Meeting*, 2013, pp. 1-5.

[36] S. D. A. Fletcher, P. J. Norman, K. Fong, S. J. Galloway, and G. M. Burt, "High-speed differential protection for smart DC distribution systems," *IEEE Trans. Smart Grid*,

vol. 5, no. 5, pp. 2610-2617, 2014.

[37] J.-D. Park and J. Candelaria, "Fault detection and isolation in low-voltage DC-bus microgrid system," *IEEE Trans. Power Deliv.*, vol. 28, no. 2, pp. 779-787, Apr. 2013.

[38] D. Wang, A. Emhemed, G. Burt, and P. Norman, "Fault analysis of an active LVDC distribution network for utility applications," Proce. *51st Int. Univ. Power Eng. Conf.*, 2016, pp. 1-6.

[39] S. Dhar, R. K. Patnaik, and P. K. Dash, "Fault detection and location of photovoltaic based DC microgrid using differential protection strategy," *IEEE Trans. Smart Grid*, pp. 1-1, 2017.

[40] N. Eghtedarpour and E. Farjah, "Control strategy for distributed integration of photovoltaic and energy storage systems in DC micro-grids," *Renew. Energy*, vol. 45, pp. 96-110, Sep. 2012.

[41] Duong Minh Bui, Keng-Yu Lien, and Shi-Lin Chen, "Investigate dynamic and transient characteristics for islanded/grid-connected operation modes of microgrid and develop a fast-scalable-adaptable fault protection algorithm," Proce. *12th IET Int. Conf. Dev. Power Syst. Prot.*, 2014, p. 8.1.4-8.1.4.

[42] C. Yuan, M. A. Haj-ahmed, and M. S. Illindala, "Protection strategies for medium-voltage direct-current microgrid at a remote area mine site," *IEEE Trans. Ind. Appl.*, vol. 51, no. 4, pp. 2846-2853, Jul. 2015.

[43] M. Carminati, S. Grillo, L. Piegari, E. Ragaini, and E. Tironi, "Fault protection analysis in low voltage DC microgrids with PV generators," Proc. *Int. Conf. Clean Electr. Power*, 2015, pp. 184-191.

[44] R. Majumder, M. Dewadasa, A. Ghosh, G. Ledwich, and F. Zare, "Control and protection of a microgrid connected to utility through back-to-back converters," *Electr. Power Syst. Res.*, vol. 81, no. 7, pp. 1424-1435, 2011.

[45] H. Hooshyar and M. E. Baran, "Fault analysis on distribution feeders with high penetration of PV systems," *IEEE Trans. Power Syst.*, vol. 28, no. 3, pp. 2890-2896, 2013.

[46] A. P. Moura, J. A. P. Lopes, A. A. F. de Moura, J. Sumaili, and C. L. Moreira, "IMICV fault analysis method with multiple PV grid-connected inverters for distribution systems," *Electr. Power Syst. Res.*, vol. 119, pp. 119-125, 2015.

[47] C. M. Franck, "HVDC circuit breakers: a review identifying future research needs," *IEEE Trans. Power Deliv.*, vol. 26, no. 2, pp. 998-1007, 2011.

[48] M. K. Bucher and C. M. Franck, "Fault current interruption in multiterminal hvdc networks," *IEEE Trans. Power Deliv.*, vol. 31, no. 1, pp. 87-95, 2016.

[49] M. Monadi, C. Gavriluta, A. Luna, J. I. Candela, and P. Rodriguez, "Centralized protection strategy for medium voltage DC microgrids," *IEEE Trans. Power Deliv.*, vol. 32, no. 1, pp. 430-440, 2017.